2016

Analysis of Sensor Coil Implemented in Maxwell-Wien Bridge Circuit for Detecting Ferrous and Non-Ferrous Particles

Kue Z. Yang
University of Akron, kzy1@zips.uakron.edu

Robert J. Veillette
University of Akron, veillet@uakron.edu

Joan E. Carletta
University of Akron, carlett@uakron.edu

Analysis of Sensor Coil Implemented in Maxwell-Wien Bridge Circuit for Detecting Ferrous and Non-Ferrous Particles

Presented to

The Faculty of The University of Akron

Kue Z. Yang

May, 2016

Abstract

This paper presents an analysis of a wear debris sensor coil implemented in a Maxwell-Wien Bridge circuit used in detecting ferrous and non-ferrous particles. The sensor coil is designed to have a diameter approximately 15 times larger than the largest particle being detected. To detect particles up to 2 mm in diameter, a coil 30 mm in diameter was constructed. Simulations of the experiment indicate that the available particles should be detectable by the sensor coil. However, experimental results indicate that the Maxwell-Wien Bridge does not detect the available particles. Further simulations are presented accounting for parasitic capacitance of the sensor coil. The results from these simulations show that large parasitic capacitance affects the behavior of the bridge. The available particles were etched into smaller particles more typical of wear debris. It is expected that for a smaller coil, the effects of parasitic capacitance will be reduced.

I. Introduction

The sensor used for this project is based on the Maxwell-Wien bridge circuit, shown in Figure 1. The Maxwell-Wien bridge circuit is a circuit used in determining an unknown inductance of a coil. By adjusting resistive and capacitive components in the bridge until the bridge output voltage, which is the difference between v_1 and v_2 in Figure 1, is zero and using known ratios, the inductance can be calculated. This project uses Flanagan's model [2] to determine the inductance perturbation as a function of the particle's radius and other physical quantities. For the model to be accurate, the coil's diameter is required to be at least fifteen times larger than the particle's diameter. [1].

The inductance of the coil is calculated using Wheeler's formula [3]. The excitation frequency used is set to the natural frequency of the bridge and can be derived from the calculated time constants. Results from a bridge simulation showed that the bridge circuit should detect 2 mm particles. However, experimental results showed that the bridge could not detect the particles. Further bridge simulations accounted for parasitic capacitance of the sensor coil. Results showed that a large parasitic capacitance will affect the behavior of the bridge.

To prepare for future experiments, the available particles were etched into smaller particles more typical of wear debris. Due to limited options in etching iron particles, only the copper particles were etched [4]. The new particle diameters ranged from 0.1 mm to 1 mm. A new excitation frequency will be selected in order to keep the sensor coil's sensitivity high as possible for a given particle size. A range of excitation frequencies appropriate for different particle sizes is given.

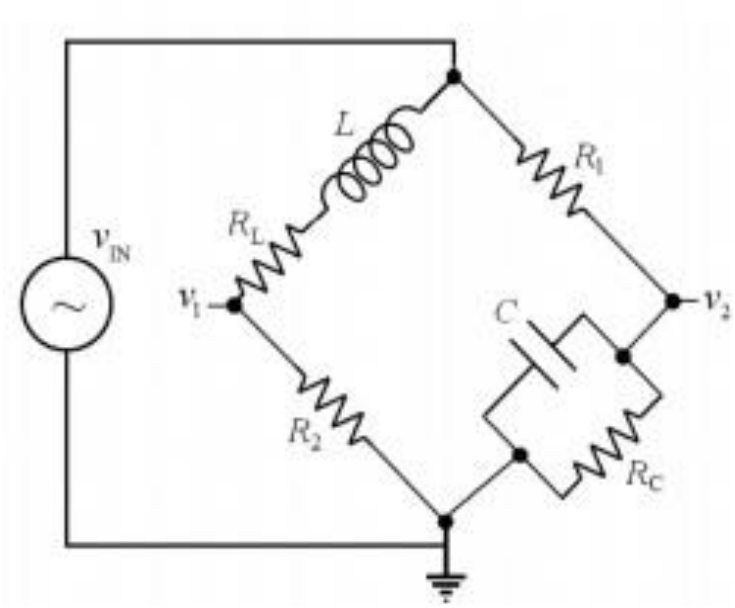

Figure 1. Maxwell-Wien bridge circuit.

II. Model Relating Particle Radius to Change in Series Resistance and Inductance

The total impedance of the sensing coil can be modeled as R + jωL, where R is the internal series resistance, ω is the excitation frequency, and L is the inductance of the coil. According to [2], change in inductance and resistance from a passing spherical particle can be calculated as

$$\Delta L = K_{CO} L \mathrm{Re}(D) \quad (1)$$

$$\Delta R = - K_{CO} L \omega \mathrm{Im}(D) \quad (2)$$

where K_{CO} is a constant depending on the physical dimensions of the coil and is calculated by

$$K_{CO} = \frac{2\left(\frac{l}{2}\right)^2\left[1 + 0.9\left(\frac{r}{l}\right) - 0.02\left(\frac{r}{l}\right)^2\right]}{\left[\left(\frac{l}{2}\right)^2 + r^2\right] l r^2} = \frac{2\left[1 + 0.9\left(\frac{r}{l}\right) - 0.02\left(\frac{r}{l}\right)^2\right]}{\left[1 + 4\left(\frac{r}{l}\right)^2\right] l r^2} \quad (3)$$

where *r* is the radius of the coil and *l* is the length of the coil. From Equations (1) and (2), it can be shown that the only constant affected by the particle's material parameters is the complex D constant. The constant D is a complex quantity determined from the physical dimensions and the composition of the particles. The expression for D is given as

$$D = \frac{[(2\mu + \mu_0)\nu I_{(-1/2)}(\nu) - [\mu_0(1+\nu^2) + 2\mu] I_{(1/2)}(\nu)]}{(\mu - \mu_0)\nu I_{(-1/2)}(\nu) - [\mu_0(1+\nu^2) - \mu] I_{(1/2)}(\nu)} \alpha^3 \quad (4)$$

where α is the radius of the particle, $I_n = I_n(\nu)$ is a modified Bessel function of order n, $\nu = (j\omega\sigma\mu)^{1/2}\alpha$, ω is the angular frequency of the applied field, σ is the particle conductivity, and μ is the magnetic permeability of the particle itself. Figure 2 shows a set of D_n ($D_n = D/\alpha^3$) function curves, plotted against α/δ, for different relative magnetic permeability. The skin depth δ for a given particle composition can be calculated as

$$\delta = \sqrt{\frac{1}{f\pi\mu_0\mu_r\sigma}} \quad (5)$$

where f is the excitation frequency and μ_r is the relative permeability of the particle [2]. Particle detection and differentiation are accomplished mainly through changes in inductance, not resistance; therefore, according to Equation (1), only the real part of D is relevant. As shown from Equation (5), the skin depth is dependent on the excitation frequency of the bridge and the material properties of the particle [1, 2].

From Figure 2, it is shown that the sensitivity for ferrous particles is better at lower frequencies while sensitivity for non-ferrous particles is better at higher frequencies. The frequency should be chosen such that there is an appropriate compromise between the sensitivity for ferrous particles and that for non-ferrous particles. In the case of iron and copper particles, the best values of α/δ fall between 10 and 1000. Table 1 lists a range of particle radii and a set of corresponding frequencies for which the values of α/δ fall within this desired range. The coil's number of turns is fixed at 12 turns and the coil's diameter is 15 times as large as the particle size when calculating the values in Table 1. Figure 3 shows the appropriate excitation frequency as a function of the particle radius. It can be seen that the appropriate frequency varies approximately as the inverse square of the particle radius [1, 2].

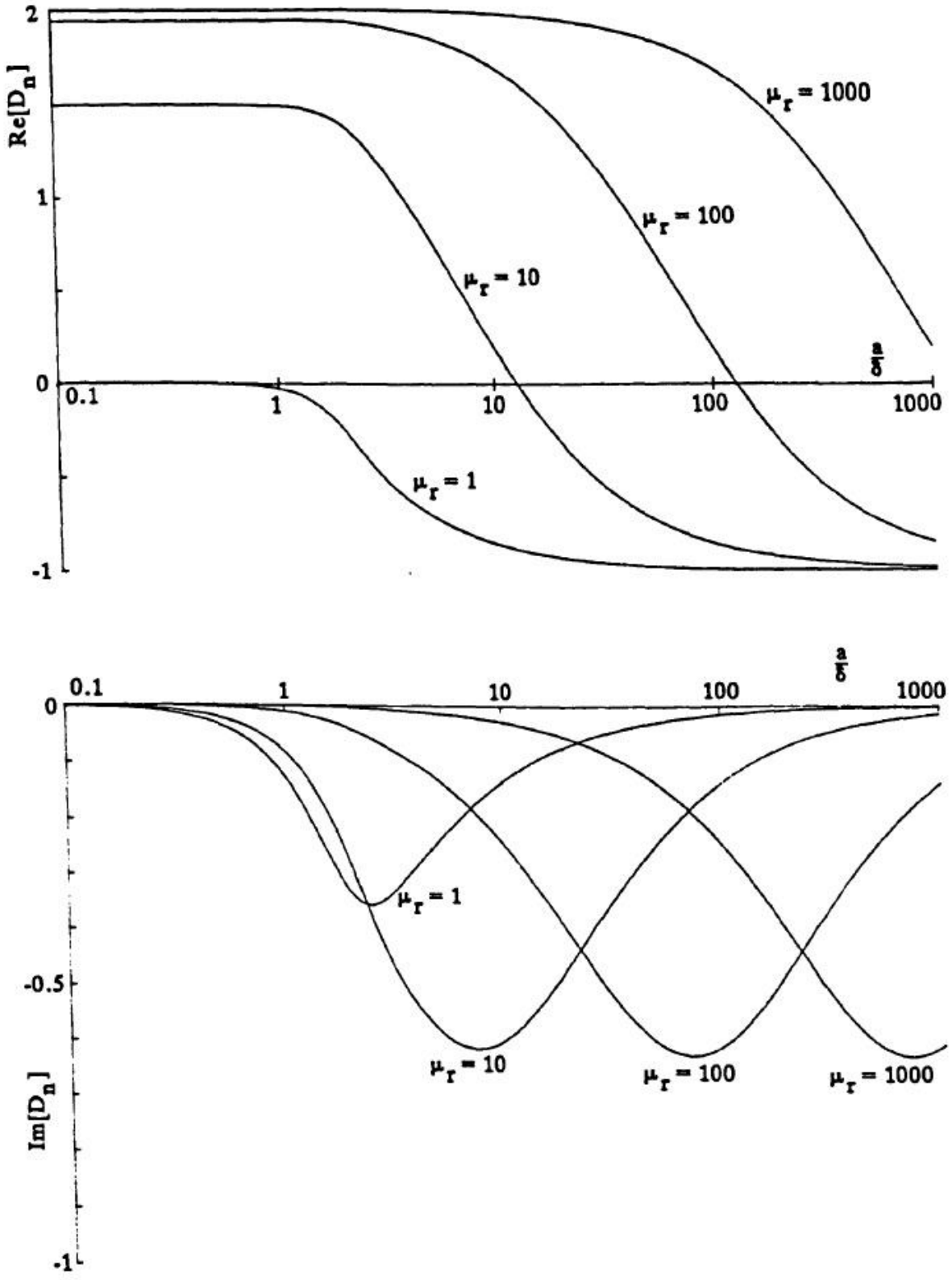

Figure 2. Plots of the real and imaginary components of Dn = D/α^3 [2].

Table 1. Particle radius α, coil diameter d, skin depth δ, and frequency chosen for corresponding D_n values.

Copper Particles				
α (μm)	d (mm)	δ (m)	Frequency (MHz)	D_n (Copper)
100	1.50	1.22E-05	30	-8.17E-01
200	3.00	1.49E-05	20	-8.88E-01
400	6.00	2.98E-05	5	-8.88E-01
800	12.0	6.67E-05	1	-8.75E-01
1600	24.0	1.33E-04	0.25	-8.75E-01
2000	30.0	2.11E-04	0.1	-8.42E-01
Iron Particles				
α (μm)	d (mm)	δ (m)	Frequency (MHz)	D_n (Iron)
100	1.50	3.00E-07	30	1.89E+00
200	3.00	3.67E-07	20	1.82E+00
400	6.00	7.34E-07	5	1.82E+00
800	12.0	1.64E-06	1	1.84E+00
1600	24.0	3.28E-06	0.25	1.84E+00
2000	30.0	5.19E-06	0.1	1.87E+00

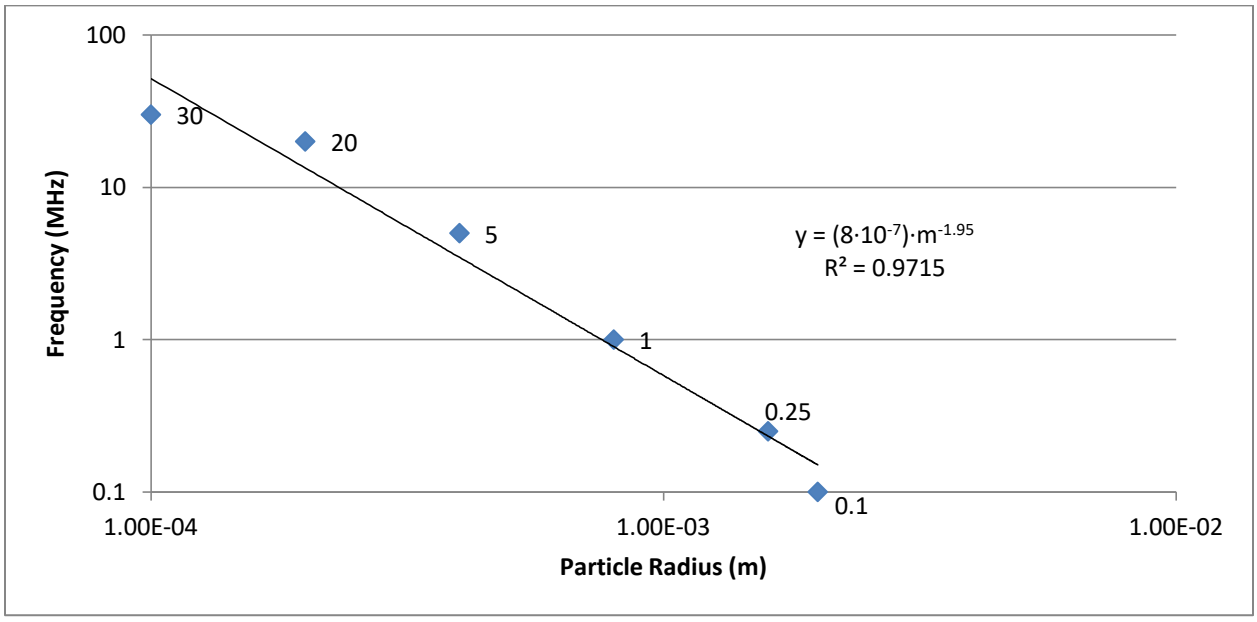

Figure 3. Frequency chosen for favorable values of D_n for a range of copper particle radii.

III. Maxwell-Wien Bridge Circuit and Sensor Coil

This section presents the equations used for the Maxwell-Wien bridge circuit and the sensing coil. The equations used to calculate the coil's inductance, the DC gain ratios and the time constants are given. The natural frequency of the bridge can be derived from the calculated time constant. The general transfer function of the Maxwell-Wien bridge circuit with and without parasitic capacitance is also given.

Inductance of the Sensor Coil:

The sensing coil is a single-layered solenoid and its inductance will be calculated using Wheeler's formula for air-core solenoids, given as

$$L = \frac{r^2 N^2}{9r + 10l} \tag{6}$$

where r is the radius, l is the length, and N is the number of turns of the coil. Both the radius and the length are in units of inches and the calculated inductance is in units of micro-Henries [3].

The Maxwell-Wien Bridge Circuit:

The Maxwell-Wien bridge circuit is shown in Figure 1. The time constants for the inductor and capacitor branches can be calculated as

$$\tau_L = \frac{L}{R_2 + R_L}, \ \tau_C = (R_C || R_1)C. \tag{7}$$

The DC gain ratios for both branches are calculated as

$$\alpha_C = \frac{R_C}{R_C + R_1}, \ \alpha_L = \frac{R_2}{R_2 + R_L}. \tag{8}$$

The bridge is considered balanced when $\tau_L = \tau_C$ and $\alpha_L = \alpha_C$ and the difference between v_1 and v_2 is zero. The general transfer function of the bridge circuit is given by

$$H(s) = \frac{V_2(s) - V_1(s)}{V_{IN}(s)} = \frac{\alpha_C}{\tau_C s + 1} - \frac{\alpha_L}{\tau_L s + 1} = \frac{(\alpha_C \tau_L - \alpha_L \tau_C)s + (\alpha_C - \alpha_L)}{(\tau_L s + 1)(\tau_C s + 1)} \tag{9}$$

where V_{IN} is the AC input source to the bridge and $V_2 - V_1$ is the AC differential voltage between the two branches of the bridge [1]. Assuming that the DC gain ratios are equal, Equation (9) is simplified to

$$H(s) = \frac{\alpha(\tau_L - \tau_C)s}{(\tau_L s + 1)(\tau_C s + 1)} \quad (10)$$

The model of the inductor with the parasitic capacitance is shown in Figure 4. The general transfer function of the bridge circuit with the parasitic capacitance is given by

$$H(s) = \frac{V_2(s) - V_1(s)}{V_{IN}(s)} = \frac{\alpha_C}{\tau_C s + 1} - \frac{\alpha_L(LC_P s^2 + 1)}{(LC_P s^2 + \tau_L s + 1)} \quad (11)$$

where C_P is the parasitic capacitance of the inductor [1]. Assuming that the DC gain ratios are equal, Equation (11) is simplified to

$$H(s) = \frac{\alpha(-LC_P s^2 + (\tau_L - \tau_C)s)}{(LC_P s^2 + \tau_L s + 1)(\tau_C s + 1)}. \quad (12)$$

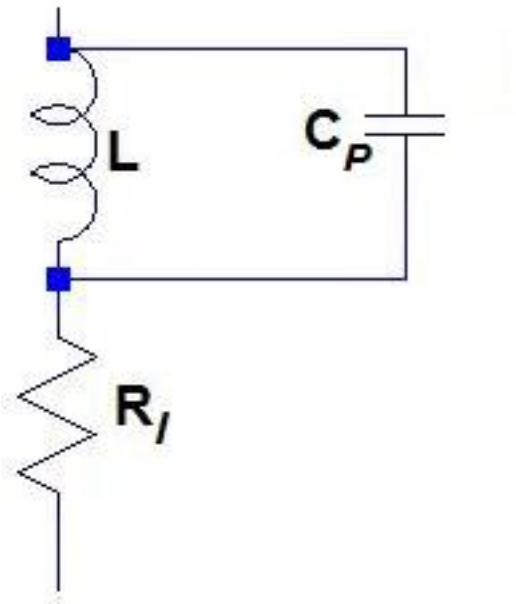

Figure 4. Inductor Model with Parasitic Capacitance.

Perturbation of the Maxwell-Wien Bridge:

The introduction of a particle into the sensor coil causes a change in the inductance and the internal resistance of the sensor coil. These changes in turn affect the time constant and DC gain ratio of the inductor branch of the Maxwell-Wien Bridge. The perturbed time constant and DC gain ratio are then given as

$$\hat{\tau}_L = \tau_L + \Delta\tau_L = \frac{L+\Delta L}{R_2+R_L+\Delta R_L}\,,\ \hat{\alpha}_L = \alpha_L+\Delta\alpha_L = \frac{R_2}{R_2+R_L+\Delta R_L}\,. \tag{13}$$

A first-order approximation of (13) can be expressed as

$$\frac{\Delta\tau_L}{\tau} = \frac{\Delta L}{L} - \frac{\Delta R_L}{R_2+R_L}\,,\ \frac{\Delta\alpha_L}{\alpha_L} = -\frac{\Delta R_L}{R_2+R_L}\,. \tag{14}$$

Applying the perturbations in (13) into (9), the transfer function of the bridge is then

$$\hat{H}(s) = H(s) + \Delta H(s) = \frac{(\alpha_c\hat{\tau}_L - \hat{\alpha}_L\tau_C)s+(\alpha_C-\hat{\alpha}_L)}{(\hat{\tau}_L s+1)(\tau_C s+1)}\,. \tag{15}$$

Ignoring the effects of $\Delta\tau_L$ in the denominator in (15), the perturbation is given as

$$\Delta H(s) = \frac{(\alpha_c\Delta\tau - \Delta\alpha_L\tau_C)s-\Delta\alpha_L}{(\tau_L s+1)(\tau_C s+1)}\,. \tag{16}$$

Assuming that $|\tau_L - \tau_C|$ is relativity smaller than either τ_L or τ_C, the frequency response of (10) at the center frequency $\omega_0 = 1/\tau$ is given as

$$H(j\omega_0) = \frac{\alpha}{2}\left[\frac{(\tau_L-\tau_C)}{\tau}\right]. \tag{17}$$

Assuming the DC gain ratios and time constants of both branches are equal and applying (14), the frequency response of (16) at the center frequency is given as

$$\begin{aligned}\Delta H(j\omega_0) &= \frac{\alpha}{2}\left[\left(\frac{\Delta\tau_L}{\tau} - \frac{\Delta\alpha_L}{\alpha}\right) + j\frac{\Delta\alpha_L}{\alpha}\right]\\ &= \frac{\alpha}{2}\left[\frac{\Delta L}{L} + j\frac{\Delta R_L}{R_L+R_2}\right]\,.\end{aligned} \tag{18}$$

Using (17) and (18), the frequency response of (15) can then be expressed as

$$\hat{H}(j\omega_0) = H(j\omega_0) + \Delta H(j\omega_0) = \frac{\alpha}{2}\left[\frac{(\tau_L-\tau_C)}{\tau} + \left(\frac{\Delta L}{L} + j\frac{\Delta R_L}{R_L+R_2}\right)\right]\,. \tag{19}$$

Maxwell-Wien Bridge Output:

In the case of a balanced bridge, the nominal transfer function will be zero. The output of a balanced bridge with perturbation is then given as

$$|\hat{H}(j\omega_0)| - |H(j\omega_0)| = \frac{\alpha}{2}\sqrt{\left(\frac{\Delta L}{L}\right)^2 + \left(\frac{\Delta R}{R_2 + R_L}\right)^2}. \quad (20)$$

From (20), the output of the bridge depends on the change in both the inductance and the resistance. The balanced bridge will need to take into account the variation in the phase of the output with respect to the excitation to differentiate between positive and negative perturbations.

On the other hand, the nominal transfer function of the imbalanced bridge with no perturbation is not zero and is given in (10). The output of the imbalanced bridge with perturbation is then given as

$$|\hat{H}(j\omega_0)| - |H(j\omega_0)| = \frac{\alpha}{2}\left[\sqrt{\left(\frac{\tau_L - \tau_C}{\tau} + \frac{\Delta L}{L}\right)^2 + \left(\frac{\Delta R}{R_2 + R_L}\right)^2} - \frac{|\tau_L - \tau_C|}{\tau}\right]. \quad (21)$$

As shown in (21), the output is still dependent on the changes in inductance and resistance, but the nominal output is not zero in this case. If the imbalance of the bridge is large enough, the output will depend primarily on the perturbation in inductance and the output will not go through zero. The positive and negative inductance perturbations can then be differentiated from the response magnitudes, without needing to take the phase into account [1, 2].

V. Frequency Response Simulations of the Maxwell-Wien Bridge

This section presents the frequency responses of two bridge circuits, one bridge circuit using a large sensor coil and another bridge circuit using a small sensor coil. The bridge component values of the bridge for both the large and small sensor coils are given in Table 2. The input signal used in the simulation is a 2 $V_{p\text{-}p}$, 2 MHz signal. The particles used in the simulations are copper and iron particles. Copper particles cause a negative perturbation in the inductance of the coil while iron particles cause a positive perturbation in the inductance of the coil. As well, both copper particles and iron particles cause a change in the resistance of the coil. However, particle detection is dependent on the change in inductance, not the change in resistance. Therefore, for these simulations, the change in the resistance of the coil is assumed to be zero [1].

The frequency responses for two bridges were simulated in LtSpice. The simulation assumes that the perturbation from the particles will cause a 0.1% change in the coil's inductance. The difference between the DC gain ratios of the two branches is approximated close to zero. The frequency responses of the bridge for both sensor coils with and without parasitic capacitance and for the balanced and imbalanced bridge are given. The parasitic capacitance, $C_{P,}$ is assumed to be 1 pF for both coils.

Table 2. Bridge Component Values for the Small and Large Coils.

	Small Coil: r = 640 μm, l = 550 μm		**Large Coil: r = 15 mm, l = 15 mm**	
Components:	**Balanced Values:**	**Imbalanced Values**	**Balanced Values:**	**Imbalanced Values**
R_1	159.154943 Ω	159.154943 Ω	159.154943 Ω	159.154943 Ω
R_C	159.154943 Ω	159.154943 Ω	159.154943 Ω	159.154943 Ω
R_2	5.9689 Ω	5.9689 Ω	91.1	91.1
R_L	5.9689 Ω	5.9689 Ω	91.1	91.1
L	950 nH	950 nH	14.5 μH	14.5 μH
C	**1 nF**	**0.975 nF**	**1 nF**	**0.975 nF**
C_P	1 pF	1 pF	1 pF	1 pF

Frequency Responses without Parasitic Capacitance:

The frequency responses of the bridge using an ideal inductor without parasitic capacitance are discussed. The frequency responses of the balanced and imbalanced bridge using the large coil are given in Figure 5 and Figure 6, respectively. The frequency responses for both the balanced and the imbalanced bridge using a small coil are given in Figure 7 and Figure 8, respectively. From Figure 5 and Figure 7, the perturbations from the copper and iron particles are shown for the balanced bridge with both perturbations having similar effect on the bridge. From Figure 6 and Figure 8, the perturbations are shown for the imbalanced bridge. The perturbations are distinct for each particle, with the copper particle causing a negative perturbation and iron particle causing a positive perturbation from the nominally imbalanced bridge response.

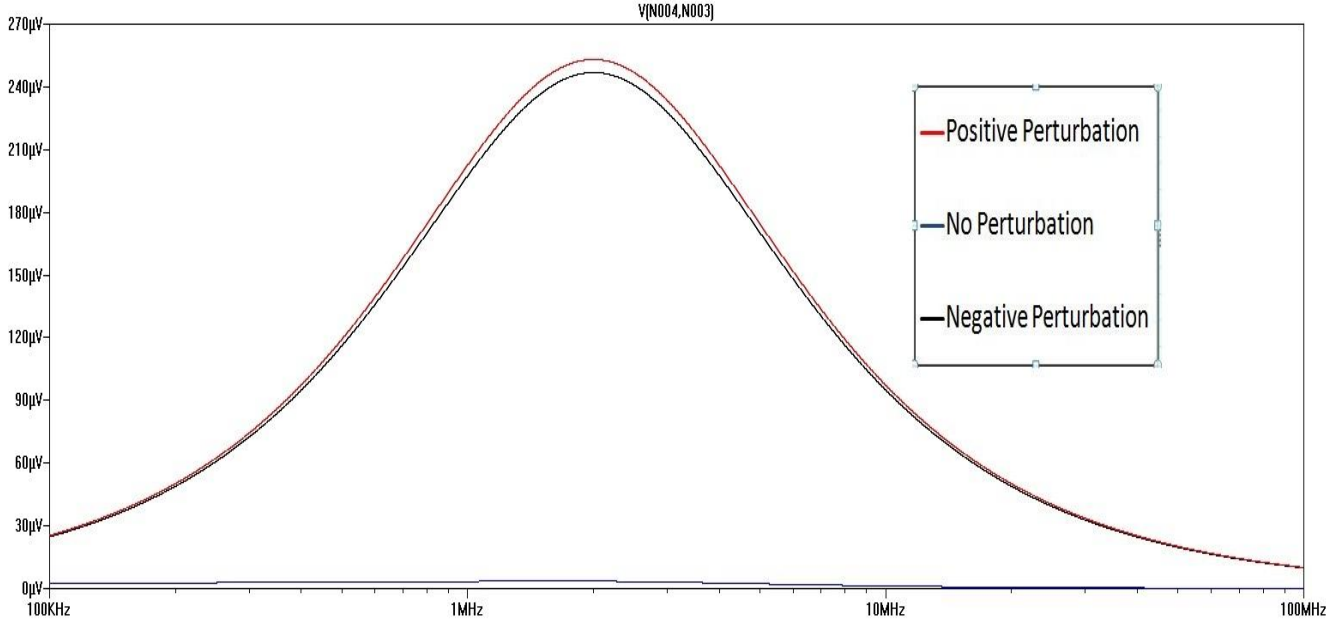

Figure 5. Frequency Response of a Balanced Bridge for a Large Coil with No Parasitic Capacitance.

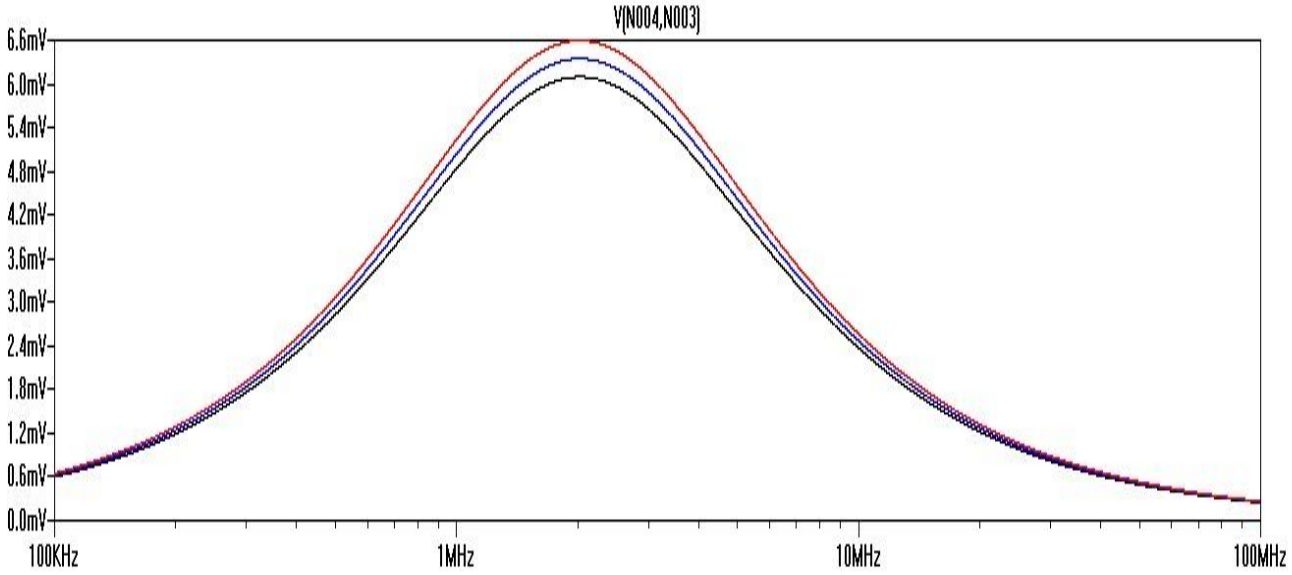

Figure 6. Frequency Response of an Imbalanced Bridge for a Large Coil with No Parasitic Capacitance.

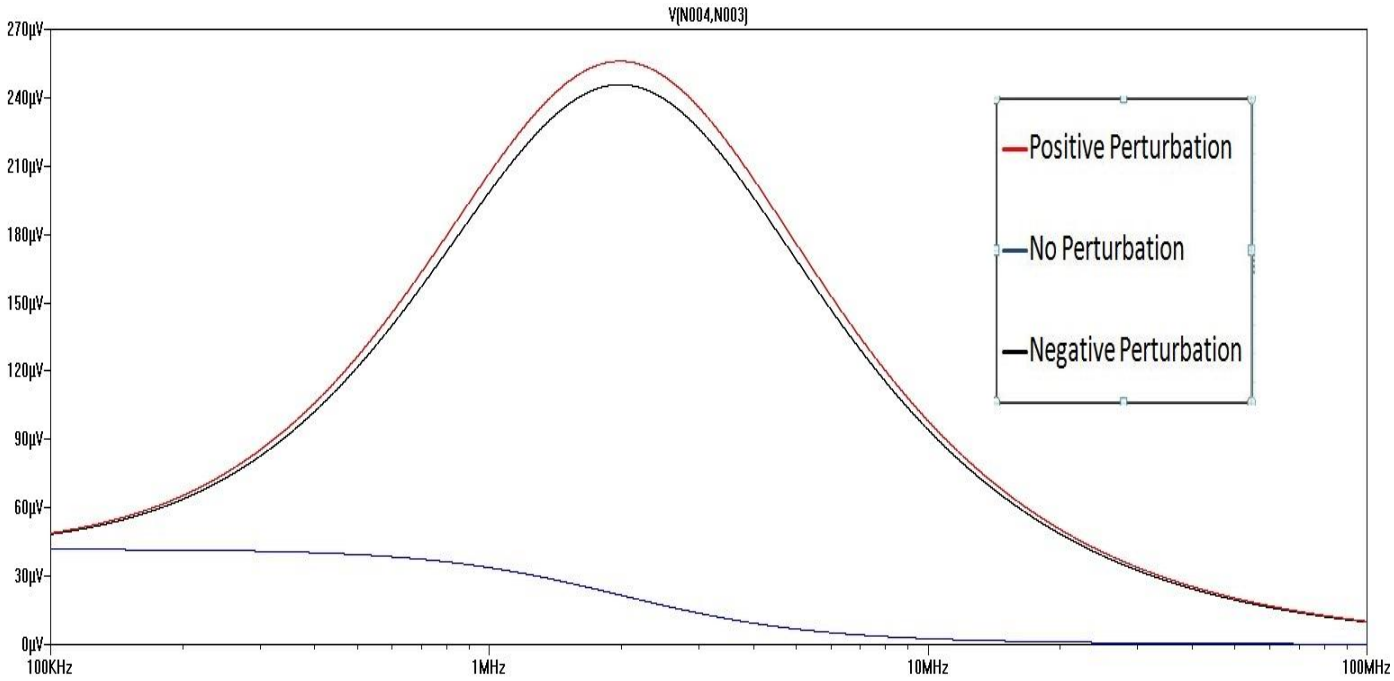

Figure 7. Frequency Response of a Balanced Bridge for a Small Coil with No Parasitic Capacitance.

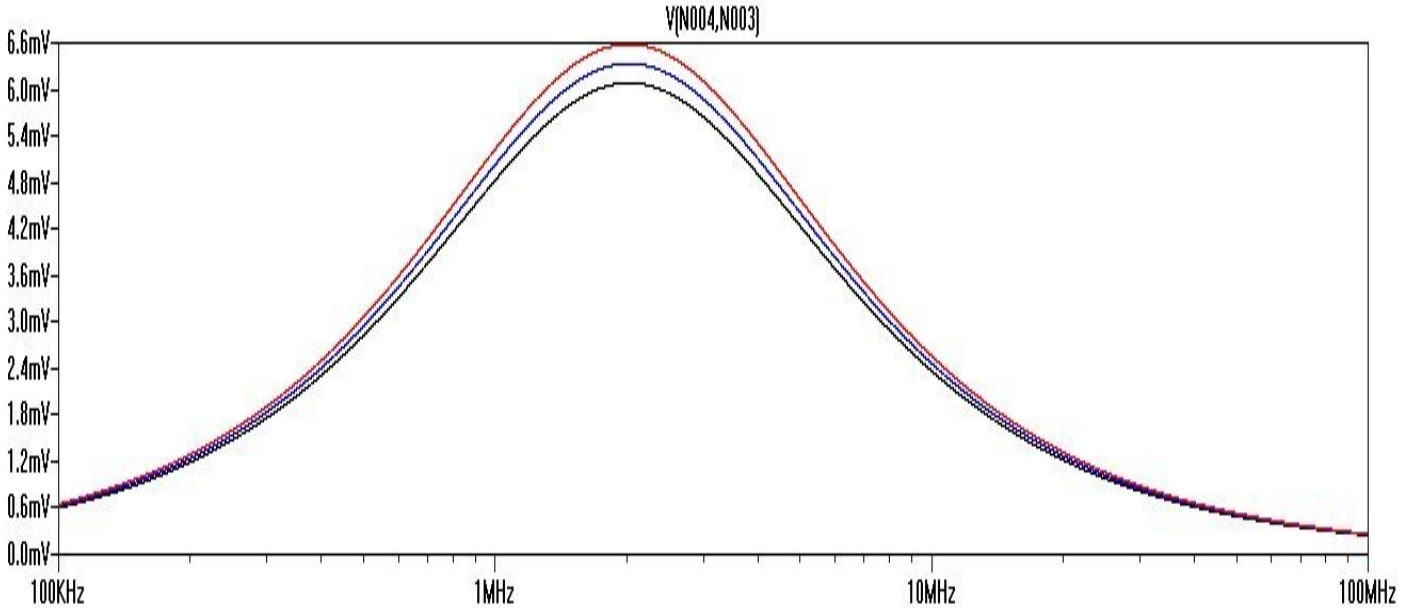

Figure 8. Frequency Response of an Imbalanced Bridge for a Small Coil with No Parasitic Capacitance.

Frequency Response with Parasitic Capacitance:

The frequency responses of the bridge using an inductor model (Figure 4) with parasitic capacitance are discussed. The frequency responses of the balanced bridge and the imbalanced bridge using the large coil are given in Figure 9 and Figure 10, respectively. The frequency responses of the balanced bridge and the imbalanced bridge using the small coil are given in Figure 11 and Figure 12, respectively. For the balanced bridge using both the large coil and the small coil, the frequency responses no longer peak at 2 MHz as they did for the cases without parasitic capacitance. In the case of the imbalanced bridge using the large coil, the frequency response also does not peak at 2 MHz. On the other hand, the frequency response of the imbalanced bridge using the small coil does peak at 2 MHz, similar to Figure 8.

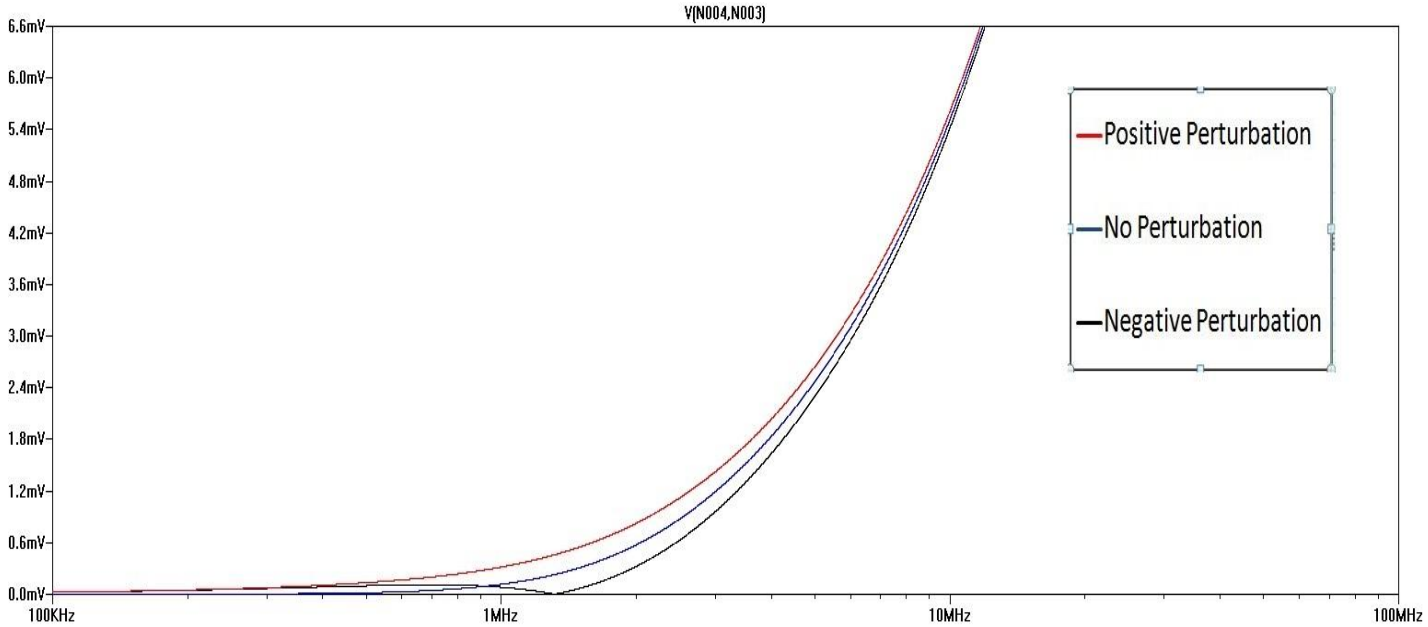

Figure 9. Frequency Response of a Balanced Bridge for a Large Coil with Parasitic Capacitance.

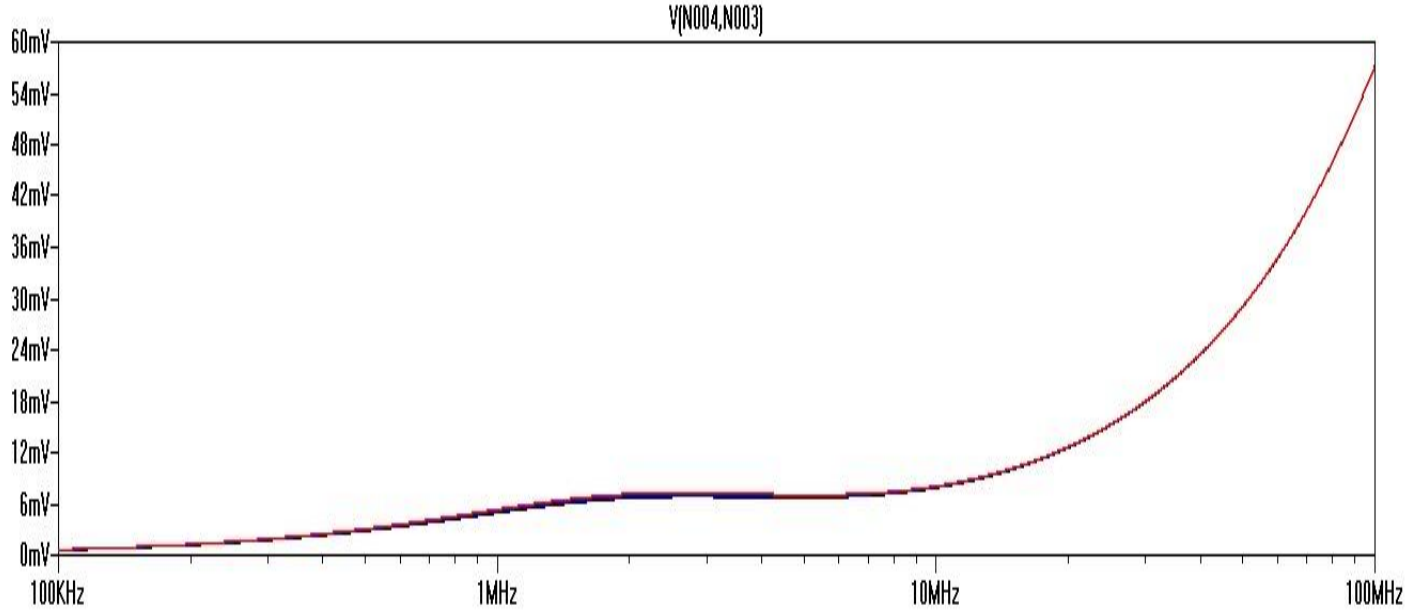

Figure 10. Frequency Response of an Imbalanced Bridge for a Large Coil with Parasitic Capacitance.

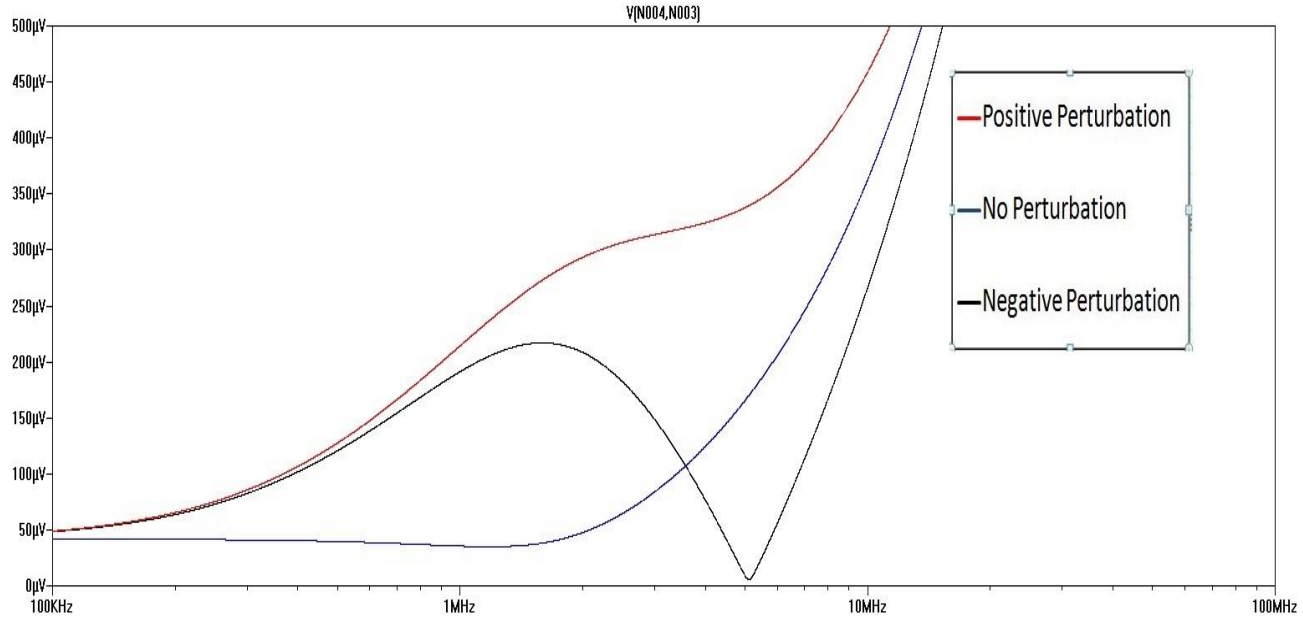

Figure 11. Frequency Response of a Balanced Bridge for a Small Coil with Parasitic Capacitance.

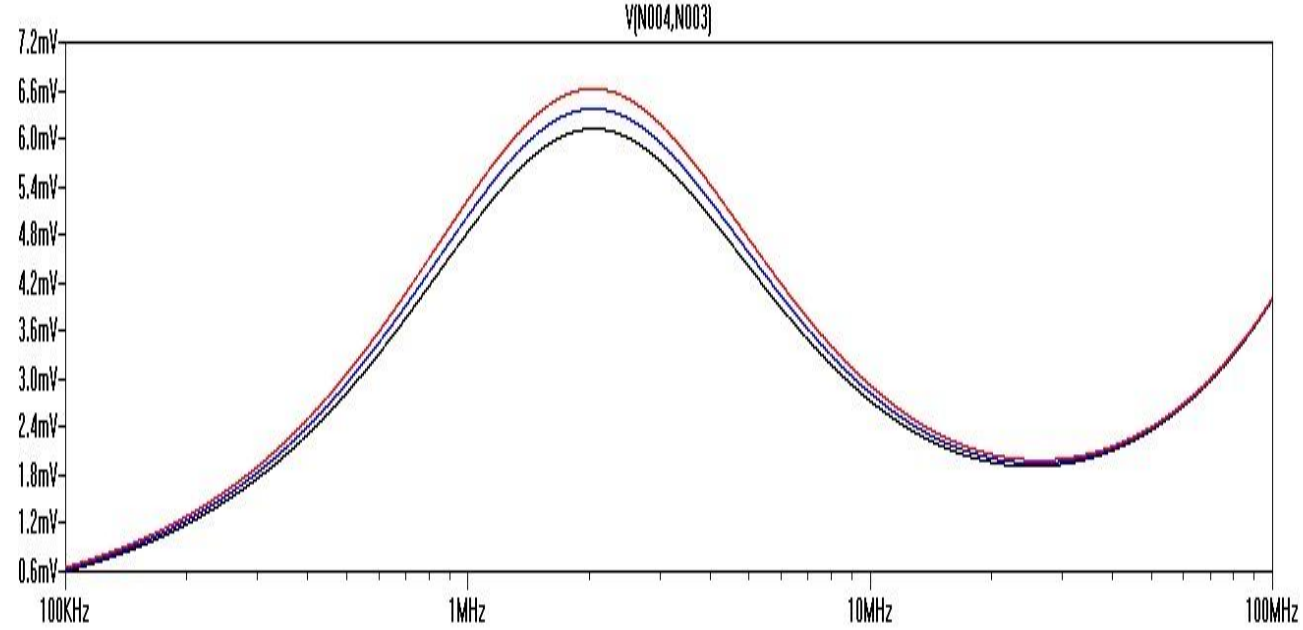

Figure 12. Frequency Response of an Imbalanced Bridge for a Small Coil with Parasitic Capacitance.

Summary of the Analysis:

For both the small coil and the large coil without parasitic capacitance, the perturbations for iron and copper particles do not vary distinctly for a balanced bridge. However, for an imbalanced bridge, the perturbations for iron and copper particles do vary distinctly. An iron particle causes a positive perturbation while a copper particle causes a negative perturbation from the nominally imbalanced bridge response. The behavior of the bridge is the same for both the small coil and the large coil.

When parasitic capacitances of the coil are taken into account, the bridge behaves differently than the bridge without parasitic capacitance. For the large coil, the frequency response no longer peaks at 2 MHz for either the balanced or the imbalanced bridge. The frequency response of the balanced bridge using the small coil no longer peaks at 2 MHz. However, in the case of the imbalanced bridge using the small coil, the frequency response does still peak at 2 MHz.

Exciting the bridge at 2 MHz using the small coil, the D_n constant for the copper particle has a value -0.1906 m^3/H and the D_n constant for the iron particle has a value 1.979 m^3/H. In other words, the bridge will be less sensitive to copper particles than to iron particles at 2 MHz. From Table 2, a more appropriate excitation frequency for the bridge using the small coil would be 30 MHz. At 30 MHz, the D_n constant for the copper particle has a value -0.786 m^3/H and the D_n constant for the iron particle has a value 1.905 m^3/H. Assuming that the parasitic capacitance of a small coil and a large coil is the same, the affect of parasitic capacitance on the bridge will be more pronounced with an increase in the excitation frequency. However, it is expected that a smaller coil will have smaller parasitic capacitance than a larger coil.

VI. Etching Copper Particles

Presently, the current available particles are 2 mm iron and copper particles. In order to experiment with a smaller coil, the particles need to be etched into smaller particles. Due to limited options in etching iron particles, only the copper particles were etched. Typically, a solution of ferric chloride is used to etch copper (e.g. etching copper off of a PCB). However, ferric chloride is expensive, and it is also a dangerous substance to handle and dispose of. An alternative etching solution is presented that is safer and easier to manage and use [4].

The Etching Solution:

The alternative etching solution presented is a mixture of household items. The items are listed as followed: Vinegar, Hydrogen Peroxide (3% concentrated), and table salt. The chemical reaction of the vinegar and hydrogen peroxide solution with the copper particles is given as

$$2(H_2O) + 2(CH_3COOH) + Cu \rightarrow 2(CH_3COO^-) + 2(Cu^+) + 2(H_20) \quad (22)$$

$$2(Cl^-) + 2(Cu^+) \rightarrow 2(CuCl) \quad (23)$$

From (22), the right hand side of the equation shows that the reaction produces copper acetate. From Equation (23), it can be shown that copper ions react with the salt, producing copper salt [4].

The solution that was used consisted of 50% vinegar and 50% hydrogen peroxide. Initially, the solution is clear and semi-transparent after placing the copper particles and the salt into the solution. The solution begins to bubble when there is a reaction between the copper particles, the salt and the vinegar and hydrogen peroxide solution. Stirring the solution helps speed up the reaction and an excess of salt in the solution is desirable, as this assures plenty of salt to use in the reaction. The solution will turn mint green, indicating that copper salt is being formed in the solution and the copper particles are being etched [4].

Etching Results:

The 2 mm copper particles were etched using a solution of 50% vinegar and 50% hydrogen peroxide and salt. Two sets of particles were etched over the course of six weeks. The first set of particles was etched over two weeks, whereas the second set of particles was etched over four weeks. The first set of etched particles ranged from 0.2 mm to 1 mm and the second set of etched particles ranged from 0.1 mm to 1 mm. The particles were measured using a millimeter ruler and magnifying glass with a magnification of 15. The etched particles may no longer be spherical and may have different length and widths.

Conclusion

Previous analysis and simulations did not take into account the effects of parasitic capacitance of the sensor coil. Further analysis and simulations were conducted in order to understand the effects of parasitic capacitance on the bridge's behavior. The results show that an imbalanced bridge is not affected as badly as a balanced bridge by parasitic capacitance. It is expected that a smaller coil will have less parasitic capacitance and the effects of parasitic capacitance will be smaller compare to large coils.

To experiment with a smaller coil, the present particles were etched into smaller particles more typical of wear debris. Reducing the particle size also requires increasing the excitation frequency in order to keep the same D_n constant. The appropriate excitation frequencies for different particle sizes and coil diameters are given. Particle sizes and the excitation frequencies should be picked such that the magnitude of D_n is large for both copper and iron particles.

Reference

[1] J. Davis, “Electronic Interface for an Inductive Wear Debris Sensor For Detection of Ferrous and Non-Ferrous Particles,” M.S thesis, Dept. Elect. Eng., Univ. of Akron, Akron, OH. 2013.

[2] I. M. Flanagan, J. R. Jordan, H. W. Whittington, “An Electronic System For Wear-Debris condition Monitoring,” Faculty of Science, Univ. Edinburgh, Edinburgh, Scotland, Mar. 1987.

[3] J. Lux. (2001). *Wheeler Formulas for Inductance* [Online]. Available: http://home.earthlink.net/~jimlux/hv/wheeler.htm

[4] Feynmaniac, “Is the Best PCB Etchant in Every Kitchen?” Internet: http://www.instructables.com/id/Is-the-best-PCB-etchant-in-every-kitchen-/?ALLSTEPS, May 2, 2014 [March 4, 2016].